BIOCHEMISTRY
including biophysical chemistry & molecular biology

Article

pubs.acs.org/biochemistry

Resonance Raman Spectroscopic Measurements Delineate the Structural Changes that Occur during Tau Fibril Formation

Gayathri Ramachandran,[†] Erix A. Milán-Garcés, Jayant B. Udgaonkar,* and Mrinalini Puranik*,[‡]

National Centre for Biological Sciences, Tata Institute of Fundamental Research, Bangalore 560065, India

Supporting Information

ABSTRACT: The aggregation of the microtubule-associated protein, tau, into amyloid fibrils is a hallmark of neurodegenerative diseases such as the tauopathies and Alzheimer's disease. Since monomeric tau is an intrinsically disordered protein and the polymeric fibrils possess an ordered cross-β core, the aggregation process is known to involve substantial conformational conversion besides growth. The aggregation mechanism of tau in the presence of inducers such as heparin, deciphered using probes such as thioflavin T/S fluorescence, light scattering, and electron microscopy assays, has been shown to conform to ligand-induced nucleation-dependent polymerization. These probes do not, however, distinguish between the processes of conformational conversion and fibril growth. In this study, UV resonance Raman spectroscopy is employed to look directly at signatures of changes in secondary structure and side-chain packing during fibril formation by the four repeat functional domain of tau in the presence of the inducer heparin, at pH 7 and at 37 °C. Changes in the positions and intensities of the amide Raman bands are shown to occur in two distinct stages during the fibril formation process. The first stage of UVRR spectral changes corresponds to the transformation of monomer into early fibrillar aggregates. The second stage corresponds to the transformation of these early fibrillar aggregates into the final, ordered, mature fibrils and during this stage; the processes of conformational conversion and the consolidation of the fibril core occur simultaneously. Delineation of these secondary structural changes accompanying the formation of tau fibrils holds significance for the understanding of generic and tau-specific principles of amyloid assembly.

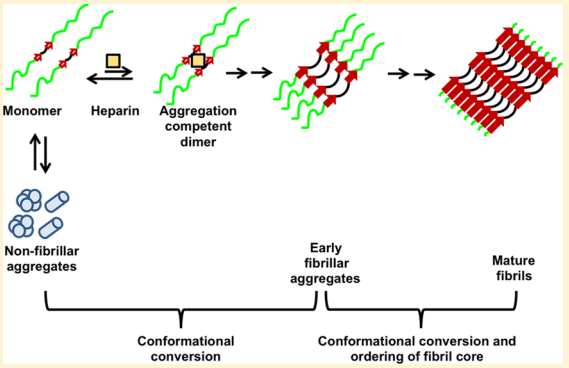

Tau is a microtubule associated protein that promotes the self-assembly of tubulin subunits and stabilizes microtubules by binding to their surfaces.[1] Tau also belongs to the class of intrinsically disordered proteins and, hence, resists folding; it exists largely as an unordered structure.[2,3] The aggregation of tau is implicated in neurodegenerative diseases such as Alzheimer's disease and the tauopathies.[4] In all of these diseases, the aggregation process is accompanied by a disorder to order transition where the predominantly disordered protein is converted to ordered amyloid fibrils with the canonical cross-β motif.[5] The mechanism of this structural transition remains an outstanding question of interest, especially from the viewpoint of the identification of inhibitory compounds that may slow or reverse neurodegeneration.

In adult neurons, tau exists in the form of six alternatively spliced isoforms ranging in size from 352 to 441 amino acid residues. These isoforms differ by the presence or absence of two inserts at the N-terminus, and by the presence of three or four imperfect repeat (R1-R4) sequences close to the C-terminus[6] (Figure 1a). These repeat sequences constitute the functional microtubule-binding domain of tau[7] (Figure 1a). Truncated repeat domain constructs have often been used as proxies for the study of tau aggregation *in vitro* since they have been shown to be the main constituent of the amyloid fibril core,[8] and their aggregation time scales are more amenable for study.[9]

In vitro, the induction of tau aggregation requires some degree of charge compensation by a ligand; commonly used inducers include polyanions such as heparin[10] or other charged molecules such as fatty acid micelles and detergents.[11,12] The mechanism of tau aggregation investigated *in vitro* largely using tools such as thioflavin T/S (ThT/ThS) fluorescence, light scattering, and electron microscopy assays, has been described primarily as ligand-induced nucleation dependent polymerization (NDP),[9,13−16] although the additional operation of secondary pathways for fibril growth has recently been demonstrated.[17] Nevertheless, the kinetics of tau aggregation has not yet been dissected using a high-resolution probe sensitive to structural transitions such as ultraviolet resonance Raman (UVRR) spectroscopy or nuclear magnetic resonance (NMR) spectroscopy.

Several high-resolution probes have, however, been applied to the study of both the initial state (tau monomer) and the final state (tau fibrils). Solution NMR spectroscopy has demonstrated the existence of residual β-strands in the tau monomer[3] (Figure 1b). Electron diffraction[18] and X-ray

Received: May 1, 2014
Revised: August 26, 2014
Published: September 18, 2014

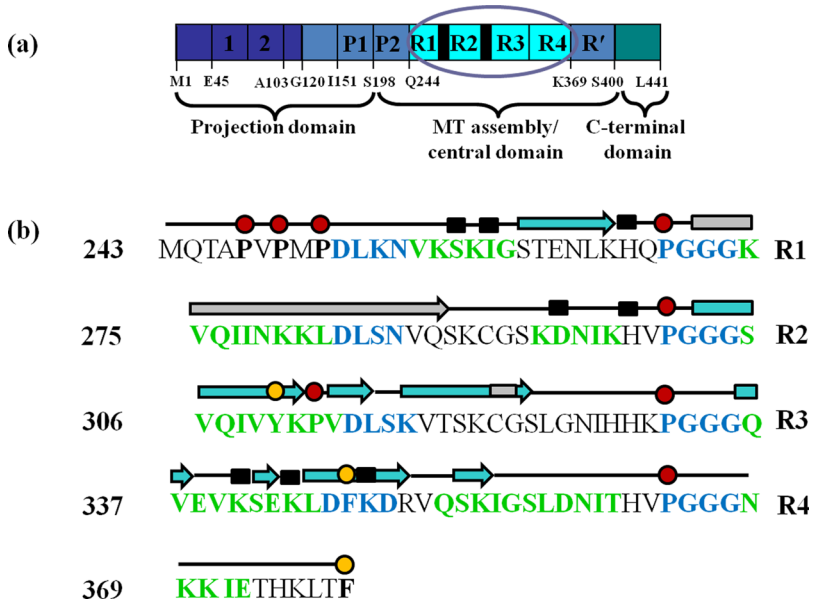

Figure 1. Important structural features of the tau monomer and fibril. (a) Domain organization of the longest tau isoform (2N4R/htau40). The N-terminal, projection domain contains two inserts labeled 1 and 2 while the central domain contains four pseudo repeat sequences (R1-R4) that constitute the fibril core and are involved in microtubule binding. P1 and P2 are proline-rich sequences; R′ refers to a sequence stretch with weak homology to the repeats. Hexapeptide motifs (PHF6* and PHF6) at the start of repeat R2 and R3, that function as important nucleating sites for tau aggregation, are labeled by black boxes. The circled region is shown in expanded form in panel b and amino acid numbers mark domain boundaries. (b) Amino acid sequence of the tau four repeat domain construct used in this study (tau4RD) and known structural features in the monomer and fibril. The tau construct used in this study comprises Q244-F378 and a 6x-His tag at the C-terminus.[14] Residues that form transient β structures in the monomer, as determined by NMR spectroscopy, are colored green.[3] Residues that possess a high propensity to populate turns in the monomer, as determined by NMR spectroscopy, are colored blue.[54] Prolines present in the sequence are marked by red circles; aromatic residues are marked by yellow circles. Structural features seen in the fibrils are shown on top of the sequence: cyan arrows mark consensus β strands as determined using EPR and ssNMR spectroscopy of both full-length and three-repeat tau constructs,[20−22,56] gray arrows and gray regions in the cyan arrows mark regions of structural heterogeneity in the β-structure,[21,56] black boxes represent sites of trypsin digestion,[55] and black lines represent linker regions that are present potentially as turns or loops.[20−22,56]

diffraction experiments[19] have shown that the tau fibril core is arranged in the cross-β motif. More recently, the application of electron paramagnetic resonance (EPR) and solid-state NMR (ssNMR) spectroscopy has shown that the β-strands in the core composed of the repeat domain, are arranged in parallel and in-register.[20,21] There are, however, disordered regions in the fibril core as well[21,22] (Figure 1b), and this existence of structural disorder within the ordered amyloid fibrils has several possible ramifications for fibril stability, growth, and structural polymorphism.[23]

A study of the kinetics of the structural transition from monomer to fibril requires the use of high-resolution probes that are sensitive to changes in secondary structure. Circular dichroism (CD) and Fourier transform infrared (FTIR) spectroscopy are probes that are commonly used to characterize secondary structure content,[24,25] but for aggregation studies, the former probe is limited by its sensitivity to scattering artifacts[26,27] while the latter is limited by its requirement of protein concentrations in the millimolar range in order to obtain data of reasonable quality.[24] Hence, both probes cannot be used to study the kinetics of fibril formation in a robust manner. On the other hand, UVRR spectroscopy is uniquely suited to studying the kinetics of aggregation since the formation of insoluble particles or a gel-like phase does not limit its usage[28,29] and data can be obtained within the micromolar concentration range. Moreover, it does not require labeling, unlike high-resolution NMR probes.[29] The utilization of UV irradiation enables selective resonance enhancement of the amide vibrational modes of the polypeptide backbone, and different secondary structures such as disordered, α-helix, and β-sheet can be distinguished.[29,30] Indeed, UVRR spectroscopy has been used successfully to study the aggregation mechanisms of both lysozyme and a model intrinsically disordered polypeptide.[28,31]

The mechanism of fibril formation by the functional, four repeat domain of tau (tau4RD) in the presence of heparin, at pH 7 and at 37 °C, was studied previously using ThT fluorescence as a probe.[14] It was shown that the pathway of aggregation involves a nucleation step in which heparin brings two tau4RD molecules together to form the aggregation nucleus, and that tau4RD monomers can also form transient, off-pathway, nonfibrillar aggregates,[14] which disappear well before the final mature tau fibrils form. Since ThT fluorescence does not distinguish between the processes of conformational conversion and fibril growth, there was the need for a probe that could directly measure changes in secondary structure and side-chain packing.

In this study, UVRR spectroscopy is utilized to study the kinetics of fibril formation by tau4RD under the same aggregation conditions as that used in the previous study.[14] An examination of the kinetics of changes in the positions and intensities of Raman bands that are sensitive to secondary structural changes suggests that these changes occur in two stages during tau fibril formation. Stage I of changes in the UVRR spectra corresponds to the formation of early fibrillar aggregates, which appear to possess a mixture of β-sheet and disordered content, with the disordered segments interspersed between the β-strands in the β-sheet. Stage II corresponds to the conversion of the early fibrillar aggregates into the final,

dx.doi.org/10.1021/bi500528x | Biochemistry 2014, 53, 6550−6565

ordered fibrils, and this process is characterized by simultaneous conformational conversion and consolidation of the fibril core. This fibril maturation process is accompanied by an increase in β-sheet content, as well as structural rearrangements within the disordered segments. It is proposed that the redistribution of disordered conformers involves the conversion of unordered conformations to either the turn or polyproline II (PPII) conformation in the segments that intersperse the β-strands in the fibril. Further, on the basis of the similarity in apparent rates measured by ThT fluorescence and by the intensity evolution of Raman bands, it appears that the fluorescence of the dye ThT largely measures the fibril maturation process.

EXPERIMENTAL PROCEDURES

Protein Expression and Purification. The expression and purification of the tau four-repeat domain (tau4RD) has been described previously.[14] The purity of the protein was confirmed using SDS-PAGE and electrospray ionization-mass spectrometry. The protein was stored at −80 °C in 25 mM Tris buffer with 50 mM NaCl (pH 7).

Buffers, Solutions and Experimental Conditions. All reagents used were of the highest purity grade available from Sigma, unless otherwise specified. At the start of the experiment, the protein was diluted to the desired concentration of 100 μM in the aggregation buffer (25 mM Tris buffer, 50 mM NaCl, 1 mM DTT, pH 7). The protein was then incubated for 2 h at 37 °C, for the reduction of disulfide-bonded dimers or compact monomers of tau4RD to free monomers by the reducing agent DTT (dithiothreitol), because tau4RD has two cysteine residues (Figure 1b), and the intramolecular disulfide-bonded compact monomer has been shown previously to be recalcitrant to aggregation.[32] Subsequently, the reaction was induced by the addition of heparin (M_r 12 000 Da, HiMedia Laboratories, India) of final concentration 37.5 μM, and measurements were made thereafter. The careful handling of aggregation reactions to ensure reproducibility has been described previously.[14]

ThioflavinT (ThT) Fluorescence Assay. The ThT assay was performed at pH 7 in 25 mM Tris buffer. For every time point, a final concentration of 1 μM aggregate and 10 μM ThT was used. Measurements were made within 30 s of addition of the protein to the assay solution, using a Fluoromax-3 spectrofluorimeter (Jobin Yvon) with the following parameters: excitation wavelength, 440 nm; emission wavelength, 482 nm; excitation bandwidth, 1 nm; and emission bandwidth, 10 nm.

Sedimentation Assay. The amount of soluble protein present in the supernatant at different times of aggregation was determined using a sedimentation assay coupled to the measurement of tyrosine fluorescence at 303 nm. Briefly, at different time points, samples were withdrawn and spun in an ultracentrifuge (Beckman Optima TL) in the TLA 100 rotor at 245 300g (75 000 rpm) for 45 min at 4 °C. The tyrosine fluorescence of the supernatant was then measured on the Fluoromax-3 spectrofluorimeter (Jobin Yvon), and the concentration of soluble protein (monomer) was determined using a standard curve.

Atomic Force Microscopy (AFM). AFM samples were made at specified times of aggregation. Briefly, 100 μL neat aliquots of the aggregation reaction were withdrawn at the designated times, applied to freshly cleaved mica (Grade V1, SPI supplies), and incubated for 2 min. The mica surface was then rinsed with 25 drops of filtered Milli-Q water, and the samples were dried under vacuum for 1 h, following which images were acquired. The time lag between removal of a sample and its application on the freshly cleaved mica surface was ∼30 s, similar to the time taken for ThT fluorescence measurements. Images of dried samples were acquired on a PicoPlus AFM instrument (Molecular Imaging, Inc.) in the noncontact mode using a ∼100 μm large scanner (Agilent Technologies). Cantilevers used were 75 kHz, 2.8 N/m with a rounding tip radius of <10 nm (Nanoworld, AG). Image acquisition parameters were scan speed = 1.0−1.5 lines/s and pixel intensity = 1024 data points/line.

Ultraviolet Resonance Raman (UVRR) Spectroscopy. The detailed UVRR setup has been described previously.[33] All resonance Raman spectra reported in this study were recorded at an excitation wavelength of 220 nm produced as the output of the fourth harmonic of a Ti:sapphire (Ti−S) laser, pumped by a Nd:YLF laser (Photonics Industries, Bohemia, NY). Raman scattering was dispersed using a monochromator (Jobin Yvon) equipped with a 3600 grooves/mm grating and recorded using a 1024 × 256 pixels, back-illuminated CCD camera (Jobin Yvon). The spectra were calibrated using the known band positions of standard solvents: cyclohexane, acetonitrile, and isopropyl alcohol.

Samples were placed in Suprasil NMR tubes that were spun about their axes to minimize photodamage. Tyrosine fluorescence of the monomer (0 h) was recorded before and after the recording of Raman spectra to ensure that there was no significant change to the monomer as a result of the acquisition conditions (Figure S1a, Supporting Information). For aggregate samples (all time points other than 0 h), a 3 mm × 3 mm PTFE magnetic bead (Bel-Art Products) was used inside the tube to ensure that the aggregates remained in suspension. The bead was seen to fragment fibrils as reported earlier.[34] ThT fluorescence of aggregate samples was recorded before and after the recording of Raman spectra to ensure that the loss of fibrillar material was less than 15%, on average (Figure S1b, Supporting Information). The typical laser power at the sample was 0.6 mW. The integrity of a sample in laser light was confirmed by comparing the spectra obtained at the first and last cycles and confirming that there was no significant difference.

All spectral processing was conducted using SynerJY (Jobin Yvon). The spectral contributions of tube and water were numerically subtracted. Each spectrum shown is the average of four fresh samples with a total exposure time of 10 min for each sample. This averaged spectrum for each time point constituted one data set. A second replicate data set was generated on a different day with an independent laser alignment, for the purpose of assessing UVRR data reproducibility. The laser stability during experiments was monitored by recording the spectrum of the external standard, sodium perchlorate (0.5 M), before and after each set of four samples recorded for one time point. The change in intensity of the 933 cm^{-1} band of perchlorate was found to be less than 4%, on average (Figure S2, Supporting Information).

Band positions and intensities were determined by fitting Lorentzian functions to the bands of the averaged spectra. Band positions were accurate to within ±2 cm^{-1} across the two independent data sets. A global fit was performed on the entire data set with the minimum number of bands that could be resolved over the entire time series. The width of a particular amide band was determined by an unconstrained fit to a time point where that band was well-defined, and this width was then constrained across all time points. The assumption that

the width of most bands does not change substantially (± 2 cm^{-1}) as a function of aggregation time was determined to be reasonable since the residuals of the fit with this width constraint in place were acceptable. The widths of the aromatic bands were also constrained. The 1003 cm^{-1} band of both L-phenylalanine and the monomer (0 h) were first fitted using unconstrained fits to determine the width of this particular band in phenylalanine present in solution versus phenylalanine present in the amide backbone of tau4RD. This difference in widths was then used to define the allowed window of expansion for the widths of all the other aromatic bands. Thus, the widths of all aromatic bands were constrained across the different time points, such that the widths were within ± 2 cm^{-1} of each other. Since the residuals of the fit were not significantly altered with this constraint in place, the width constraint for the aromatic bands was also deemed acceptable. Bands were assigned to amide and aromatic modes based on comparison with the literature.[28−30,35−46]

The intensity of a Raman band was calculated as the area under the band. The use of an external standard to plot intensities as a function of time was undertaken because it was not possible to use a salt as an internal standard. The aggregation of tau4RD is extremely sensitive to electrostatic interactions,[14,22] and the presence of even small amounts of salt alters aggregation kinetics and the nature of the spectra (data not shown). The intensities of bands were normalized to the mean intensity of the 933 cm^{-1} band of the perchlorate spectra acquired before and after each time point of aggregation (Figure S2, Supporting Information). Across the two independent data sets, the intensities were further normalized to the respective 24 h data point to allow for comparison.

RESULTS

Amyloid Fibril Formation Studied Using ThT Fluorescence and Sedimentation Assays. In previous studies of tau aggregation from our laboratory utilizing ThT fluorescence as the probe, two different constructs of the four repeat domain of tau, tau4RD and tau-K18, were used.[14,17] The apparent rate of formation of amyloid fibrils by 100 μM tau4RD in the presence of 37.5 μM heparin (HMW heparin, $M_r \approx 12$ kDa), when monitored by ThT fluorescence, has a value of 0.35 ± 0.07 h^{-1} (Figure 2a) and is therefore slow enough for UVRR measurements. The final fibrils formed by tau-K18, as assayed by AFM, FTIR spectroscopy, and hydrogen−deuterium exchange coupled to mass spectrometry (HX-MS) are similar to those formed by tau4RD,[47] and the aggregation pathways of both constructs follow the same basic NDP mechanism.[17] However, the fibril formation reaction of tau-K18 is far too fast for UVRR spectroscopic measurements and is more complex, because of the presence of an additional secondary pathway for fibril growth.[17] It is for these reasons that this first UVRR spectroscopic study of the kinetics of tau fibril formation has been carried out using tau4RD.

ThT fluorescence has been used as a quantitative probe for the formation of β-sheets in several studies of amyloid fibril formation, ever since pioneering initial studies carried out a thorough characterization of its fluorescence and binding properties.[48,49] Since ThT binds to diverse fibrils formed from diverse amino acid sequences, it is generally accepted that the dye recognizes the common structural core of all amyloid fibrils, the cross-β motif. Recent studies have determined that ThT monomers bind parallel to the long axis of the fibril surface in channels formed by aromatic residues.[50,51] Indeed, aromatic dyes such as ThT have been shown to influence fibril

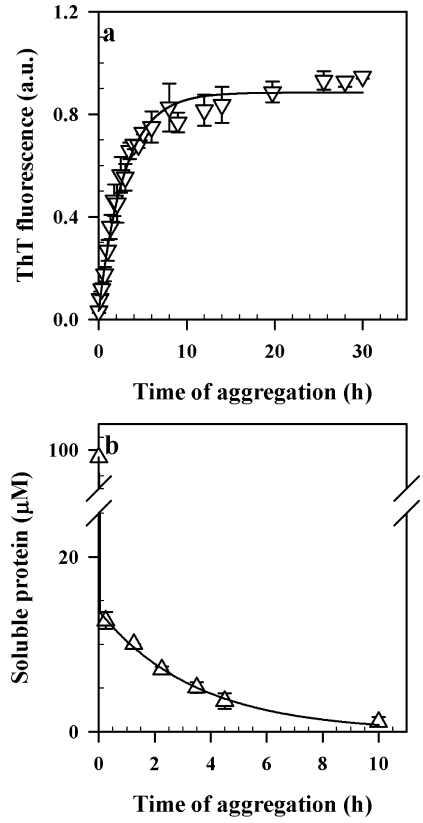

Figure 2. Kinetics of formation of amyloid fibrils by 100 μM tau4RD in the presence of 37.5 μM heparin at 37 °C and pH 7. (a) ThT fluorescence monitored kinetics. The continuous line through the data points is a least-squares fit to a single-exponential equation. (b) Sedimentation assay. The continuous line through the data points is a least-squares fit to a double exponential equation. For both plots, the error bars represent the spread in the data calculated from two or more independent experiments.

aggregation kinetics.[52] In this context, it is important to note that measurements of ThT fluorescence in this study were made by removing aliquots of the aggregation reaction and mixing with the ThT dye before the reading; ThT was not present in the aggregation buffer.

A sedimentation assay was used to quantify the amount of protein that had not formed sedimentable aggregate at different times during the aggregation reaction. The assay itself takes 45 min and hence could not report on the rate of disappearance of soluble (nonsedimentable) protein within the first hour of aggregation. But the entire aggregation process takes 10 h to complete and the sedimentation assay reports reliably on both the rate and extent of loss of soluble protein from 1 to 10 h. The kinetic curve of loss of soluble protein from 1 to 10 h is well described as a single exponential process (Figure 2b), and extrapolation of the kinetic curve to zero time indicates that about 90% of the soluble protein has disappeared before any measurement can be made by the sedimentation assay. Hence, 90% of the soluble protein disappears in a "burst phase" within the measurement dead-time of 45 min, and the remaining 10% disappears in an observable phase with an apparent rate of 0.29 ± 0.02 h^{-1} (Figure 2b). This apparent rate of disappearance of soluble protein is similar to the rate of evolution of ThT fluorescence (Figure 2a). The small difference between the rate measured by ThT fluorescence (0.35 h^{-1}) and that measured by the sedimentation assay (0.29 h^{-1}) may be

dx.doi.org/10.1021/bi500528x | Biochemistry 2014, 53, 6550−6565

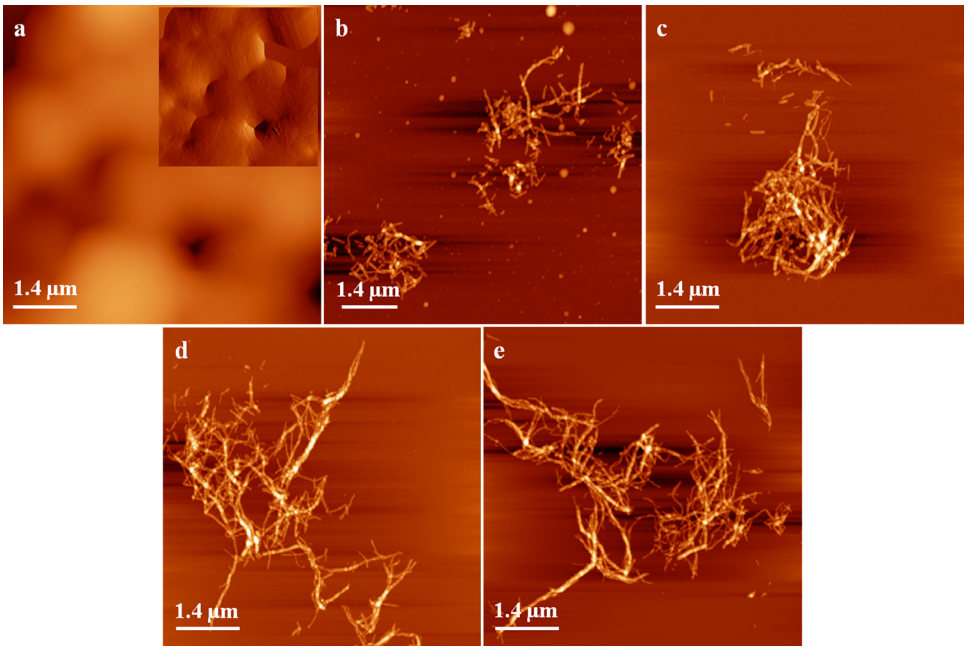

Figure 3. AFM images of structures formed at different times of aggregation. Images were acquired at (a) 5 min, (b) 1 h, (c) 3 h, (d) 10 h, and (e) 24 h of aggregation. All images are in the topography format. The inset of image a also shows the same image in the amplitude format. The scale bar in all images corresponds to 1.4 μm. The Z scale for images b through e corresponds to 75 nm; that for image a corresponds to 4 μm.

because the sedimentation assay takes 45 min to complete at each time point of aggregation; hence, the difference is not considered to be significant.

At 10 h, the amount of soluble protein present in the aggregation reaction is 1.12 ± 0.55 μM (Figure 2b). This value corresponds to the critical concentration for the aggregation of tau4RD that was determined previously for the identical aggregation conditions.[14] Hence, it appears that the major fraction of the soluble protein present at the end of the reaction is monomer. The existence of a critical concentration for aggregation is in line with expectations from the aggregation mechanism of this protein, which has been shown to be ligand-induced NDP.[9,13−15]

Morphology of Aggregates Formed at Different Times of Aggregation. Atomic force microscopy (AFM) images acquired at different times of aggregation illustrate the types of structures formed during the time course of tau4RD aggregation (Figure 3). Very early during the aggregation reaction (5 min), huge amorphous aggregates are seen to have formed (Figure 3a, see inset also), and no fibrillar aggregates are observable. These aggregates disappear quickly: at 1 h of aggregation, mostly fibrillar aggregates are visible (Figure 3b). No large nonfibrillar aggregates are seen (Figure 3b), and the few small spherical aggregates seen at 1 h are likely to be the dissociation products of the early nonfibrillar aggregates (Figures 3a,b). Hence, the AFM data suggest that the aggregates found by the sedimentation assay to be formed by 90% of the protein at 1 h of aggregation are predominantly fibrillar in nature.

The fibrillar aggregates that are first seen at 1 h of aggregation are found mainly in small clumps (Figure 3b). The fibril clumps are found to be bigger at longer times of aggregation (Figure 3). It was possible to measure the heights of individual fibrils found at the periphery of clumps. The fibrils possess heights of ∼10 nm, on average, at the time they are first observed by AFM imaging (1 h), and they do not increase in height over the time course of aggregation from 1 to 10 h (data not shown). Because the fibrillar aggregates are found to form clumps under the conditions of AFM imaging, it is difficult to determine conclusively the extent, if any, to which the fibrils grow in length from 1 to 10 h. At 10 h of aggregation, the ThT fluorescence signal has saturated (Figure 2a), indicating that the fibrils have become structurally mature at this time.

No change in fibril morphology is apparent even from 10 to 24 h of aggregation (Figures 3d,e). Hence, measures from four independent probes, namely, ThT fluorescence, sedimentation assay (Figure 2), AFM (Figure 3), and FTIR spectroscopy (Figure S3, Supporting Information) concur that the fibrillization process is largely complete by 10 h, since no further significant change in signal is visible from that time onward.

It should be noted that the time course of aggregation monitored by ThT fluorescence measurements, as well as by the sedimentation assay from 1 h onward, is described well by single exponential kinetics (Figure 2). This observation suggests that the number of fibrillar aggregates that are present during the aggregation time course from 1 h onward is roughly constant. If the fibril number was increasing or decreasing, the fibrillization rate would reflect these changes in the number of sites available for monomer addition by accelerating (at least until monomer was depleted) or decelerating as the reaction progressed. The constant number concentration of fibrils is a reasonable consequence of the model proposed earlier[14] to explain the role of heparin in inducing tau aggregation. In that model, the number of heparin-induced aggregation-competent dimers, from which fibril growth proceeds, becomes fixed early during aggregation because of the initial tight binding of heparin to monomeric tau to form the dimer.[14]

UVRR Spectra of the Monomer and Final Fibril. High-resolution NMR and EPR spectroscopic studies of the monomeric repeat domain construct of tau demonstrate that the majority of residues in the monomer exist in an aperiodic, disordered conformation reminiscent of an unordered structure.[3,20,53]

dx.doi.org/10.1021/bi500528x | *Biochemistry* 2014, 53, 6550−6565

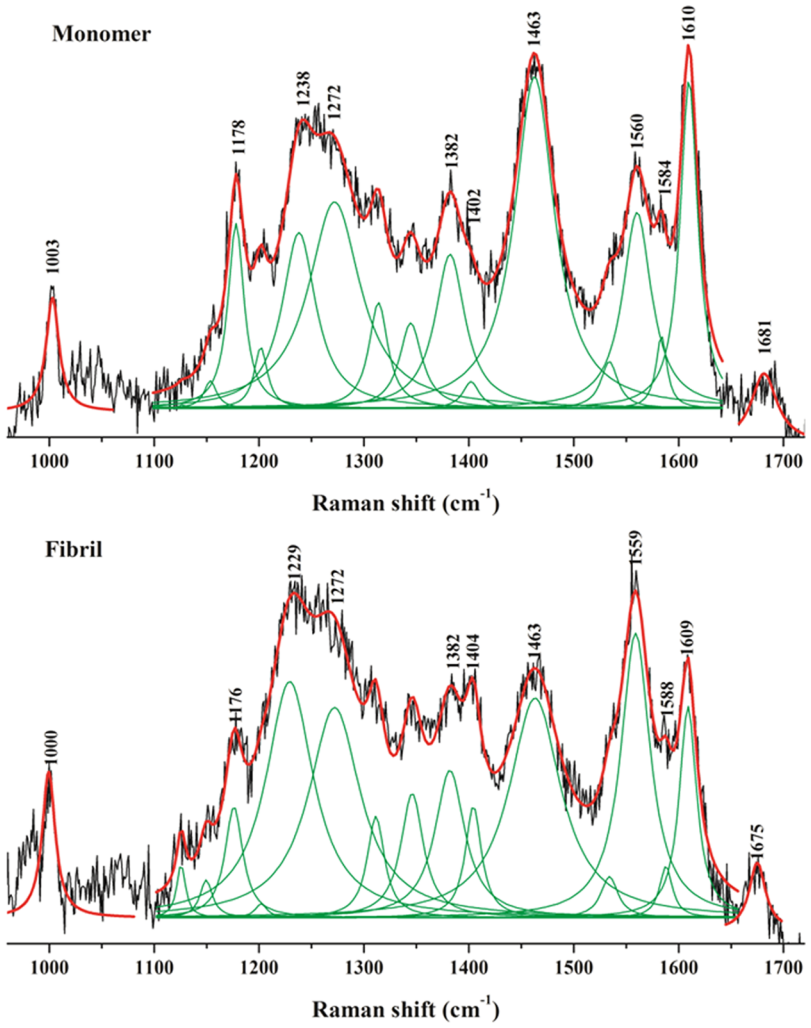

Figure 4. UVRR spectra of monomer (0 h) and fibril (24 h) acquired with Raman excitation at 220 nm. Spectra were deconvoluted by fitting to a sum of Lorentzian functions. Lorentzian decompositions are shown as green lines, and the sum of Lorentzian bands is shown as the red solid overlay. The UVRR spectrum of the monomer at 0 h was acquired in the absence of heparin.

However, short stretches of residual β-structure and β-turn conformations are also present, detected by means of combined measurements of secondary chemical shifts, J couplings and residual dipolar couplings[3,53,54] (Figure 1b). These NMR spectroscopic measurements have shown that even the highest β-structure content seen for a stretch of ~10 residues in the repeats R2 and R3 (Figure 1b), populate transiently, only 22% and 25% of the time, respectively.[3,53] On the other hand, the core of the mature tau fibril is composed of ordered β-sheets and disordered loops or turns[20−22,55,56] (Figure 1b). The loops or turns are known to connect the β-strands that constitute the parallel, in-register β-sheet[20−22,55,56] (Figure 1b). These high resolution studies set the stage for UVRR spectroscopic characterization of the kinetics of structural transition from monomer to fibril, during which there is an increase in both β-sheet and turn content at the expense of a decrease in unordered content.

The UVRR spectra of native tau4RD monomer (0 h, acquired in the absence of heparin) and the final mature fibril (24 h), recorded at 220 nm excitation wavelength are shown in Figure 4. The UVRR spectra are composed of amide vibrational modes (amide I, amide II, amide III, and C_α−H bending/amide S), an imide II mode (X-Pro), and aromatic modes (tyrosine and phenylalanine).[43] Previous pioneering studies that recorded the UVRR spectra of poly(L-glutamic acid) and poly(L-lysine) in different conformations (unordered, α-helix, β-sheet) at 218 nm[57,58] and the UVRR spectra of *N*-methylacetamide at wavelengths ranging over 238, 217, 210, 200, and 192 nm[59,60] have already demonstrated that Raman excitation at ~220 nm is within the resonance/preresonance regime and that it produces enhancement of bands corresponding to the amide vibrations. Additionally, in the case of tau4RD, the absence of tryptophan and the presence of only one tyrosine and two phenylalanine residues (Figure 1b) allow reliable information from the amide backbone to be obtained with excitation at 220 nm. Importantly, upon excitation at 220 nm, there are no significant aromatic bands underneath the amide III envelope (Figure 4), and this lessens the complications that may potentially arise during the analysis of the Raman bands. Thus, although the choice of 220 nm as the excitation wavelength might be unwise for other proteins that contain tryptophan,[43,61] for this first study of tau fibril formation using UVRR spectroscopy, the selection of 220 nm as the excitation wavelength has resulted in well-resolved spectra of sufficiently good quality (Figure 4).

The interpretation of the UVRR data obtained in this study has relied on the correlation between spectral characteristics

dx.doi.org/10.1021/bi500528x | *Biochemistry* 2014, 53, 6550−6565

Table 1. Amide Bands Associated with Secondary Structures and Their Assignments

amide band	band position (cm^{-1})	secondary structure	mode assignment
amide I (Am I)	1660−1682	disordered	C═O stretching[28−30,35,39−42]
	1670−1675	β-sheet	
amide II (Am II)	1548−1561	disordered	out-of-phase combination of N−H in-plane bending (NH ib) and C−N stretching (CN s)[29,30,39,41,42,62]
	1550−1564	β-sheet	
amide III (Am III)	1240−1279	disordered	in-phase combination of NH ib and CN s[28−30,35,38,39,41,42]
	1220−1230	β-sheet	
C_α−H bending (C_α−H/amide S)	1380−1390	disordered	C_α-H bending coupled to N−H bending[29,30,37,39,41,42,46]
	1395−1406	β-sheet	

and secondary structures established by various detailed studies that have predominantly used excitation wavelengths shorter than 220 nm (see Table 1). The use of these references for assignments of Raman bands remains valid, however, since the positions of Raman bands depend only on the ground state geometry of the molecule and not on the excitation wavelength. Although the Raman cross-section is known to become larger as the excitation wavelength is decreased from 220 to 200 nm, the quality of spectra obtained with excitation at 220 nm in this study matches the quality of spectra obtained with shorter wavelength excitation for several other studies of protein aggregates.[28,31,35,39,62,63]

The important amide modes that are associated with changes in secondary structure are listed in Table 1. The important amide band positions obtained following deconvolution of the monomer (0 h) and the mature fibril (24 h) spectra are listed in Table 2 and shown in Figure 4. These band positions were

Table 2. Amide Band Positions in the Monomer and Fibril

amide band	band position in monomer (0 h) (cm^{-1})	band position in fibril (24 h) (cm^{-1})
amide I	1681	1675
amide II	1560	1559
amide III_3	1238	1229
C_α−H bending	1382, 1402	1382, 1404

determined by performing an iterative global fit to all of the spectra collected at all of the different time-points, with the minimal number of bands required to fit the entire data set (see Experimental Procedures). This is important to note, especially with reference to the fitting of the crowded amide III region (Figure 4).

The vibrations of the tyrosine and phenylalanine residues contribute distinct Raman bands at 1178 and 1610 cm^{-1}[136] (Figure 4). The 1003 cm^{-1} band (Figure 4) arises solely from the phenylalanine ring breathing mode.[36] The 1463 cm^{-1} band (Figure 4) arises from the C−N stretching vibration of the X-Pro peptide bond, which is known to be sensitive to the effects of hydrogen bonding at the X-Pro carbonyl.[44,45]

The spectrum of the native tau protein at 0 h (Figure 4) is consistent with that expected for a disordered protein since the main band positions obtained from the fit (Figure 4, Tables 1 and 2) corresponds to the disordered conformation. Indeed, CD, FTIR, EPR, and NMR spectra of the native monomer had shown previously that the protein is, by and large, intrinsically disordered.[3,20,64] The disordered conformations of monomeric tau4RD would include the unordered conformation and possibly the PPII conformation and β-turns. The Raman band positions for the PPII conformation are known from the UVRR spectra of model peptides[29,38,41,65] proven to adopt the PPII conformation by NMR and vibrational CD measurements.[66] Unfortunately, there is considerable overlap in the Raman band positions assigned to the PPII and other disordered conformations,[29] and for disordered proteins such as tau4RD, it is not possible to distinguish the PPII conformation from other disordered conformations. This is not surprising since PPII may be thought of as a subclass of the disordered/coil library.[67] In the case of the monomeric repeat domain of tau, NMR studies have also not detected any PPII conformation.[3,53] Hence, the disordered Raman band positions in the monomer are interpreted to reflect the family of disordered conformers consisting of unordered structures and β-turns.

The asymmetric shape of the C_α−H bending/amide S Raman band observed in the tau4RD monomer spectrum indicates the possible presence of residual β-structure (Figure 4, Table 1). However, none of the Raman band positions (Figure 4) correspond to those expected for type I and II β-turns.[30,61] There is evidence from previous work, however, that the β-turns cannot be distinguished from other categories of secondary structure with Raman excitation at 206.5 nm and that this is possible only when UVRR spectra are acquired at 197 nm.[29,30] It is thus possible that β-turns that are expected to be present in the tau monomer cannot be resolved with Raman excitation at 220 nm either. Residual β-structure and β-turn conformations in tau4RD have been detected previously only by NMR spectroscopy,[3,53,54] and a Raman optical activity study of the full-length tau protein.[68]

The spectrum of the final fibril at 24 h (Figure 4) is consistent with that expected for structures that are enriched in β-sheets since the main band positions obtained from the fit (Figure 4, Tables 1 and 2) correspond to the β-sheet conformation. The final fibril also possesses disordered regions as indicated by the presence of Raman bands (1272, 1382 cm^{-1}) that serve as signatures of the disordered conformation (Figure 4, Table 1). This is consistent with other studies that have indicated that the mature tau fibril contains both ordered β-sheets and disordered loops or turns connecting the β-strands that compose the β-sheet[21,22,55] (Figure 1b).

UVRR Spectra Acquired at Different Times of Aggregation. The sedimentation assay shows that soluble protein disappears in two stages during aggregation (see above). At the end of stage I, at 1 h of aggregation, 90% of the protein was found to exist in aggregated form, and only 10% of the protein as soluble protein or soluble protein−heparin complexes (Figure 2b). AFM images of the aggregating protein indicate that the dominant aggregate present at 1 h of aggregation is fibrillar in nature (Figure 3b). To characterize the fibrillar aggregate at the end of stage I, as well as the fibrillization process during stage II, UVRR spectra were acquired at different times of aggregation, recorded using excitation at 220 nm (Figure 5). Since even at the earliest time of aggregation (1 h) at which a

dx.doi.org/10.1021/bi500528x | Biochemistry 2014, 53, 6550−6565

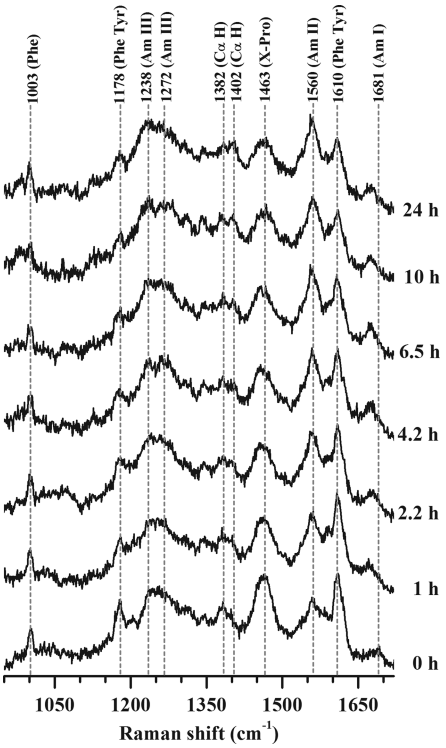

Figure 5. UVRR spectra acquired with Raman excitation at 220 nm at different times of aggregation of 100 μM tau4RD in the presence of 37.5 μM heparin, at pH 7 and at 37 °C. The dashed lines through the spectra indicate important bands. The band position labels correspond to the 0 h data. The UVRR spectrum of the monomer at 0 h was acquired in the absence of heparin.

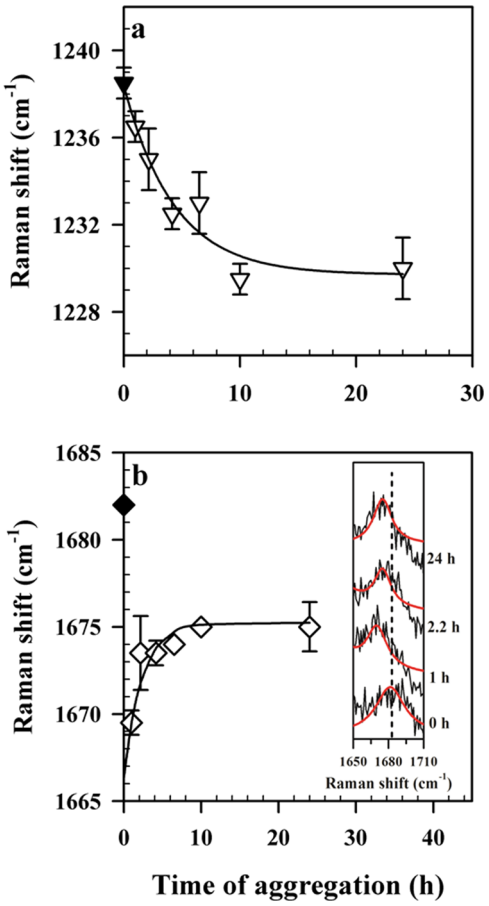

Figure 6. Changes in band position as a function of aggregation time. (a) Change in the position of the Am III_3 band. (b) Change in the position of the Am I band. The inset shows the UVRR spectra of the Am I region for four representative time points. The dashed black line in the inset represents the position of the Am I band at 0 h and the red continuous lines are least-squares fits to a sum of Lorentzian functions. For both plots, the error bars represent the spread in the data calculated from two independent experiments. In both plots, the 0 h data point is represented using a closed symbol and the continuous lines through the data points are lines drawn by inspection, intended to serve as guides for the eye.

UVRR spectrum could be recorded (see below), only 10% of the protein remains soluble and nonfibrillar in nature, the contribution of any soluble protein, whether complexed with heparin or not, to the UVRR spectra collected at and after 1 h would be small. Changes in the UVRR spectra therefore reflect conformational changes accompanying either the initial binding of heparin or the subsequent aggregation process. Changes in both band positions and intensities were seen to occur as a function of aggregation time (Figure 5). This is expected since the tau4RD monomer is intrinsically disordered, and aggregation results in the formation of fibrils with ordered β-sheets.[69] The specific bands listed in Table 2 were used to understand the kinetics of structural transition from monomer to fibril.

The changes in Raman band positions and intensities during fibril formation in the presence of heparin were found to occur in two stages (Figures 6 and 7). While the kinetic curves for some of the changes extrapolate back at $t = 0$ to the values expected for the monomer in the absence of heparin (Figures 6a and 7b), the kinetic curves for some of the changes do not (Figures 6b and 7a,c). Since the first Raman spectrum of aggregating protein was collected at 1 h of aggregation, it appears that changes in the Raman spectra occur in two stages: some within the first hour of aggregation, within the 1 h "burst phase" identified by the sedimentation assay, and some that accompany the formation of mature fibrils from 1 h onward.

It should be noted that both in the sedimentation assay and in the measurement of UVRR spectra, the burst phase of approximately 1 h arises because of the time taken for the measurements. In measuring kinetics, it is necessary that the time required for data acquisition be short compared with the time constant (characteristic time) of the process being studied. For proper analysis of the UVRR spectra, it was necessary that the spectra be collected over a sufficiently long time period to ensure that they were of acceptable quality. Hence, it was not possible to collect UVRR spectra at different times during the 1 h duration of stage I and thereby to temporally dissect events occurring during stage I. It was possible only to obtain the UVRR spectrum of the product of the 1 h "burst phase" at the end of stage I. Thus, the differences in the UVRR spectra obtained at the beginning and end of stage I report on the cumulative structural changes that occur during stage I but do not temporally resolve these changes.

The UVRR spectrum at the beginning of stage I is that of monomer in the absence of any heparin. The UVRR spectrum at the end of stage I is that of 90% of the protein that has been shown by the sedimentation assay to be aggregated and by AFM to be fibrillar. There are two possibilities about when the changes in the UVRR spectra occur during stage I. The changes could occur immediately upon the initial binding of heparin to

dx.doi.org/10.1021/bi500528x | *Biochemistry* 2014, 53, 6550−6565

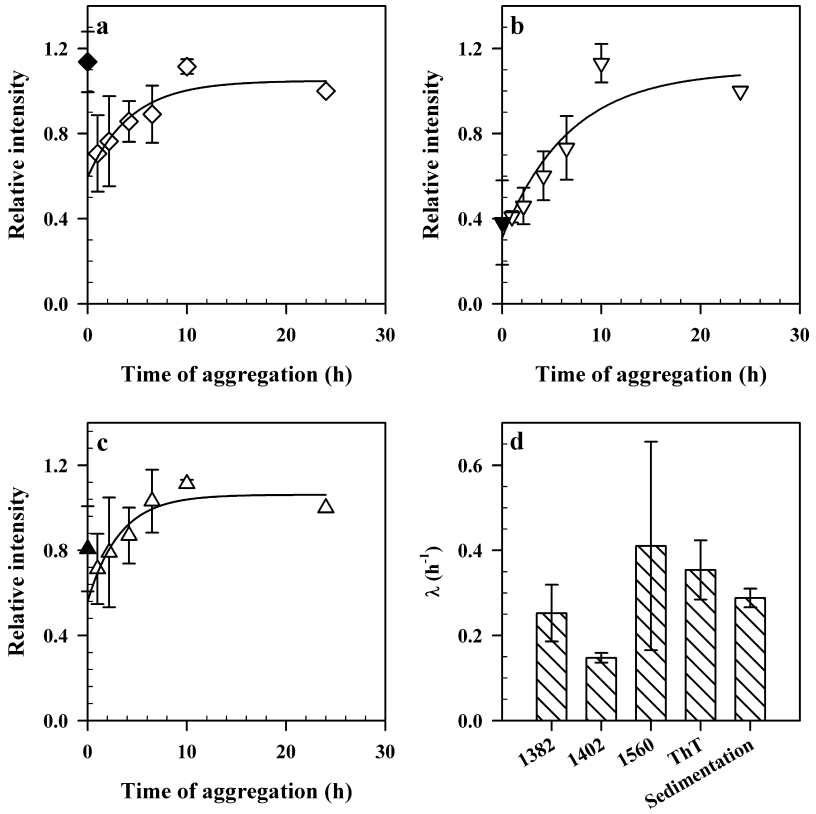

Figure 7. Intensity changes of important UVRR bands as a function of aggregation time and a comparison of apparent rate constants of aggregation measured by different spectroscopic probes. Intensities of (a) 1382, (b) 1402, and (c) 1560 cm^{-1} bands are plotted versus the time of aggregation. Intensity was measured as the area under the band, relative to that of the external standard perchlorate, and normalized to the 24 h data point. The continuous line through the data points is a least-squares fit to a single-exponential equation; for plots a and c, the 0 h data point (represented by a closed symbol) is excluded from the fit. (d) Apparent rate constants of aggregation (denoted by λ) measured by the change in intensity of UVRR bands (1382, 1402, and 1560 cm^{-1}) and by the ThT fluorescence and sedimentation assay are plotted as bar graphs. The apparent rate constants for each of the UVRR bands were compared independently, using the nonparametric Kruskal–Wallis test, to the other two apparent rate constants, and they were found to not be significantly different ($p > 0.05$). For all plots, the error bars represent the spread in the data calculated from two (for UVRR bands) or more (other probes) independent experiments.

tau to form a tight 1:1 complex.[70] It has been shown that under aggregation conditions identical to those used in the current study, such binding occurs rapidly and enables the formation of an aggregation-competent dimer, which then serves as a template for the addition of monomers leading to fibril growth.[14] Alternatively, the changes could occur subsequently, as 90% of the protein with heparin bound assembles to form fibrillar aggregates at the end of stage I. It should be noted that although the final, mature tau fibrils appear to have insignificant amounts of heparin bound,[14,55,71] it is likely that some heparin remains bound to tau during the first hour of aggregation.

Previous studies have shown that the binding of heparin to the repeat domain of tau extends and stabilizes the residual β-structure thereby maintaining a compact, aggregation-prone conformation.[53,72,73] It is thus possible that changes in UVRR signatures that occur during stage I may arise from these initial heparin–tau interactions. It might have been possible to delineate changes that occur as a consequence of the initial binding of heparin to tau, from those that occur subsequently as 90% of the protein forms fibrillar aggregates at the end of stage I by the use of aggregation-incompetent mutant tau that cannot form fibrils.[21,74] But the "antiaggregant" mutant tau proteins have been shown to form amorphous aggregates instead of fibrils in the presence of heparin.[21] Moreover, single molecule force spectroscopic studies have shown that the "antiaggregant" tau protein adopts alternative conformations not adopted by the wild-type, which additionally, are not perturbed upon the addition of heparin.[73] These observations hence preclude the use of aggregation-incompetent mutant tau for the purpose of delineating changes in UVRR signatures during stage I.

It should be noted that virtually all changes in the UVRR spectra from 1 h onward are describable by single exponential kinetics (Figures 6 and 7) with rates that approximately match the kinetics of ThT fluorescence evolution (Figure 7d). As discussed above for the single exponential change in both ThT fluorescence and loss of soluble protein, the observation that all UVRR spectral signatures change with single exponential kinetics from 1 to 10 h, suggests that the fibril number remains approximately constant from 1 h onward. The observation of single exponential kinetics is also expected when the rate-limiting step during aggregation is conformational change and not growth of fibrils.

Change in Position of Specific Amide Bands as a Function of Aggregation Time. Band positions were obtained following deconvolution as described in Experimental Procedures. Two bands change position as a function of aggregation time, a sub-band of the Am III called Am III$_3$ and Am I (Figure 6 and Table 2).

Amide III. The Am III region contains several sub-bands, of which the lowest frequency Am III$_3$ band is the most sensitive

dx.doi.org/10.1021/bi500528x | *Biochemistry* 2014, 53, 6550–6565

marker of secondary structure conformation.[38,43,75] Bands found in the 1240−1279 cm^{-1} region have been assigned to the disordered conformation, while bands found in the 1220−1230 cm^{-1} region have been assigned to the β-sheet conformation (Table 1). In this study of tau aggregation, the Am III_3 band changes position from 1238 cm^{-1} in the monomer to 1230 cm^{-1} in the fibril (Figure 6a, see fits in Figure 4; Table 2), consistent with a change in conformation from disordered to β-sheet.

Fibrils formed by lysozyme and the Aβ 34−42 peptide where the core is arranged in an antiparallel β-sheet, show Am III_3 bands centered at 1225 and 1222 cm^{-1}, respectively.[35,39] On the other hand, Aβ 1−40 fibrils in a parallel β-sheet conformation show two characteristic Am III_3 bands at 1214 and 1233 cm^{-1}.[35] Based on these observations, a reasonable conclusion based on the Am III_3 band position of the final tau fibrils (1230 cm^{-1}), is that the tau4RD fibrils possess a parallel β-sheet core. This is consistent with previous interpretations of the FTIR spectra of tau4RD fibrils, which show a characteristic band at ∼1626 cm^{-1} (Figure S3, Supporting Information). This coupled with the absence of a second band at ∼1680 cm^{-1} (Figure S3, Supporting Information) has been interpreted to mean that the fibril core is composed of a parallel β-sheet.[14,64,76] Indeed, this is completely consistent with other high-resolution structures of the tau fibril; both EPR and ssNMR studies concur that tau fibrils are composed of a parallel in-register β-sheet.[20,21]

While the change in position of the Am III_3 band reflects a change in conformation as monomer transforms into fibril, a more informative exercise would have been to determine the actual rate of conformational conversion. It is interesting to note that the characteristic time of change in the Am III_3 band position appears similar to the evolution of ThT fluorescence (Figures 6a and 2a). A robust method to determine the rate of conformational conversion would have been to examine how the relative areas of the two bands (1238 and 1230 cm^{-1}) change as a function of aggregation time. However, the present data set does not allow the resolution of two bands in the Am III_3 region (see fits in Figure 4).

Amide I. The Am I band also changes position in disordered conformations (1660−1682 cm^{-1})[42,77] with respect to β-sheet conformations (1670−1675 cm^{-1}).[28,30,39−42] During tau fibril formation, the Am I band downshifts from 1681 cm^{-1} for the monomer in the absence of heparin at 0 h to 1670 cm^{-1} for predominantly (90%, see Figure 2b) aggregated fibrillar protein in the presence of heparin at 1 h (Figure 6b, see inset also). This reflects a change in conformation from disordered in the monomer to β-sheet in the aggregated fibrillar protein at 1 h at the end of stage 1 of aggregation (Table 1). It should be noted that the monomer begins to aggregate immediately upon addition of heparin,[14] and it is therefore not possible to obtain the spectrum of monomeric tau4RD in the presence of heparin.

Over the time scale of 1 to 24 h, the Am I band further changes position from 1670 to 1675 cm^{-1} (Figure 6b, see inset also), which is the band position that has been annotated for the cross-β core of lysozyme and Aβ fibrils.[28,35,39] Moreover, the width of the Am I band in the 24 h fibrils is also approximately half that of the width of the Am I band in the 0 h monomer (data not shown), a trend similar to that seen for the cross-β core of lysozyme fibrils.[39] The characteristic time of change in the Am I band position from 1670 cm^{-1} at 1 h to 1675 cm^{-1} at 24 h appears to be similar to the characteristic time of evolution of ThT fluorescence during aggregation (Figures 6b and 2a). This change in band position is interpreted to be a reflection of the ordering or consolidation of the fibril core, which could arise from either the packing of β-strands within a β-sheet or the packing of the β-sheet bilayer that comprises the cross-β core of fibrils.

Change in Intensity of Specific Amide Bands As a Function of Aggregation Time. Intensities of Raman bands were determined as areas under the fitted peaks, relative to the area of the 933 cm^{-1} band of perchlorate, the external standard (see Experimental Procedures). Further, the kinetic curves were normalized to the respective 24 h data point, across the two independent data sets. These plots of change in intensity were primarily used to infer the kinetics of structural transition. Since the Raman scattering cross sections differ for different secondary structures (disordered, α-helix, β-sheet) at a particular wavelength and across wavelengths, the intensities of different Raman bands cannot be compared, *per se*, to draw inferences about the relative populations of various conformations.[43] The rate of change in intensity can be used, however, to infer the rate of change in the population of a particular conformer, and this has been the primary interpretation of this study.

Figure 7 shows the changes in intensity as a function of aggregation time of three important Raman bands that serve as signatures of protein secondary structure, namely, 1382 and 1402 cm^{-1} (C_α−H bending) and 1560 cm^{-1} (Am II) (Figure 7a−c, Table 1). It is to be noted that since the concentration of fibrillar aggregates is as high as 90% as early as 1 h into the aggregation reaction (Figure 2b), these plots of change in intensity from 1 h onward reflect the conformational changes that occur within the fibrils as their structures mature. Figure 7d compares the apparent rate constants measured by the different spectroscopic probes utilized in this study.

The 1382 cm^{-1} Raman band is an important marker for the disordered conformation.[28−31,41,46] An important observation of this work is that the intensity of this band decreases in value (Figure 7a) as the monomer in the absence of heparin at 0 h predominantly transforms into the early fibrillar aggregates seen at the end of stage I of aggregation (Figures 2b and 3b). This decrease in intensity reflects a change in conformation, presumably induced by heparin binding during the first few seconds of aggregation (see above). Conformational change is also indicated by the change in the Am I band position from 1681 cm^{-1} for the monomer in the absence of heparin at 0 h to 1670 cm^{-1} for the early fibrillar aggregates that have formed at 1 h (Figure 6b). Further, the width of the Am I band also changes from ∼32 to ∼21 cm^{-1} (data not shown), indicating that some level of compaction occurs when monomer in the absence of heparin at 1 h transforms into the early fibrillar aggregates in the presence of heparin at 1 h.

Subsequent to this dip in intensity, there is an increase in the intensity of the 1382 cm^{-1} Raman band as a function of aggregation time (Figure 7a). This increase in intensity is interpreted to reflect the evolution of disordered regions as the early fibrillar aggregates observed at 1 h transform into the final, mature fibrils observed at 24 h (Figure 3). Indeed, both ssNMR and EPR studies of tau fibrils indicate the existence of disordered regions in the fibril core formed by the repeat domain (see Figure 1b).[20,21] In this context, it is important to note that although the relative intensities of the monomer at 0 h and the fibril at 24 h appear similar for the 1382 cm^{-1} Raman band (Figure 7a), this is a fortuitous coincidence and does not indicate that the monomer and fibril possess the same amount of disordered content. The similar relative intensities of these bands also do not indicate that the final fibrils have degraded to

dx.doi.org/10.1021/bi500528x | *Biochemistry* 2014, 53, 6550−6565

monomer since fibril formation is essentially irreversible and the amount of soluble monomer present at the end of the aggregation reaction, as determined by the sedimentation assay, is ~1% (Figure 2b).

Figure 7b shows the change in intensity of a bonafide β-sheet marker, the 1402 cm^{-1} band.[30,39,41,78] The evolution of this Raman band appears to reflect the ordering or consolidation of the fibril core in a manner similar to the change in Am I band position from 1 to 24 h (Figure 6b). Like the 1382 cm^{-1} Raman band, the 1560 cm^{-1} band (Figure 7c) too shows a dip in intensity as monomer in the absence of heparin at 0 h, transforms into the early fibrillar aggregates in the presence of heparin at 1 h, at the end of stage I of aggregation. The assignment of the 1560 cm^{-1} band has been debated. While some groups assign the band to the disordered or PPII conformation,[29] others have assigned it to the β-sheet conformation.[30,39,62] The pattern of change in intensity of the 1560 cm^{-1} band during tau fibril formation parallels not only that of the 1382 cm^{-1} band (Figures 7a,c) but also that of another disordered Raman band, 1272 cm^{-1} (data not shown). Hence, it appears that the 1560 cm^{-1} band either monitors the disordered conformation or a mixture of β-sheet and disordered conformations.

Figure 7d compares the apparent rates of change measured by the different spectroscopic probes employed in this study. The apparent rates measured by the each of the three Raman bands were compared independently to the apparent rates measured by ThT fluorescence and the sedimentation assay, using the nonparametric Kruskal–Wallis test, and the rates were found to not be significantly different from each other, at the 95% level of confidence ($p > 0.05$) (data not shown). Although the evolution of the 1402 cm^{-1} Raman band appears to be slightly slower than that of the other biophysical probes (Figure 7d) and this rate being slower would be consistent with a physical scenario where fibril core consolidation follows the process of conformational conversion measured by the other probes, the statistical treatment of the data do not allow us to make this conclusion, especially given the spread in the data.

Change in Intensity of an Aromatic Band as a Function of Aggregation Time. Figure 8 shows the change in intensity of the 1610 cm^{-1} band (Y8a, F8a, ring C–C stretch)[46] as a function of aggregation time. The 1610 cm^{-1} band contains contributions from both the single tyrosine residue (Y310) and the two phenylalanine residues (F346 and F378) (Figure 1b). Since the absolute cross sections of the corresponding bands of tyrosine and phenylalanine (1617 and 1606 cm^{-1}, respectively) are not very different at 218 nm,[79] it seems that the change in the intensity of the 1610 cm^{-1} band reflects changes in both the tyrosine and phenylalanine residues.

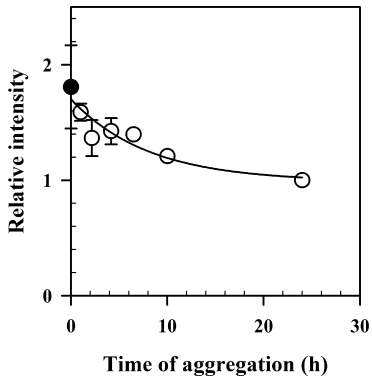

Figure 8. Intensity change in the 1610 cm^{-1} band as a function of aggregation time. Intensity was measured as the area under the band, relative to that of the external standard perchlorate, and normalized to the 24 h data point. Each error bar represents the spread in the data calculated from two independent experiments. The continuous line through the data points is intended to serve as a guide for the eye.

The decrease in intensity of the 1610 cm^{-1} band is a measure of the change in the solvent environment surrounding the aromatic residues. Previous work that has examined the dependence of the tryptophan and tyrosine Raman cross sections in model proteins on solvent environment, has demonstrated that a decrease in water content red-shifts the tyrosine and tryptophan absorption bands at ~220 nm.[80] This red shift in both the absorption band and the Raman excitation profile will result in a decrease in the intensity of the 1610 cm^{-1} band. Arguing backward from this inference, the decrease in intensity of the 1610 cm^{-1} band seen in this study can therefore be attributed to a burial of these residues as the transition occurs from monomer to fibril. Since the change in intensity appears to occur with a characteristic time similar to the evolution of the 1402 cm^{-1} band (Figure 8, Figure 7b), it appears likely that this decrease in intensity also arises from the ordering of the fibril core. The annealing of β-strands within a β-sheet, or the pleating of β-sheets to form the fibril core is likely to affect side-chain packing[56] and, hence, the solvent accessibility of these aromatic residues.

There is substantial evidence in the literature implicating the sequence stretch containing Y310 called PHF6 (^{306}VQIVYK^{311}) (Figure 1), as the primary nucleating motif in tau fibril formation.[74] In addition, a study that examined the tau protein for other amyloidogenic sequences outside of the two canonical hexapeptide motifs (PHF6 and PHF6*) found that peptides containing the two phenylalanine residues (Ac^{343}KLDFK^{347} and Ac^{375}KLTFR^{379}; see Figure 1b) were amyloidogenic as well.[81] Further, ssNMR and HX-NMR studies have shown that both Y310 and F346 form parts of two different β-strand structures in the fibril core[20−22] (Figure 1b). The observation from this work that the tyrosine and phenylalanine residues become buried during aggregation is in agreement with these previous results.

Changes in Proline Residues during Tau Aggregation. A recent study that compared residues found in disordered regions of fibrils to those found in ordered regions determined that the disordered regions are significantly more enriched in proline.[23,82] The locations of the eight proline residues in tau4RD are shown in Figure 1b. The 1463 cm^{-1} band in the acquired UVRR spectral time series (Figure 5) corresponds to imide II (C–N stretching vibration of X-Pro peptide bond).[30,44,45] The position of this band, which is known to be sensitive to hydrogen bonding at the X-Pro carbonyl, is consistent with the position seen in unfolded proteins and indicates strong hydrogen bonding to solvent molecules.[44−46] Since the position of the X-Pro band remains unchanged as a function of aggregation time (Figure 5), this indicates that the proline residues remain in disordered regions in both the monomer and the fibril. Incidentally, the intensity change of the 1463 cm^{-1} band shows a similar pattern of dip and rise (Figure S4, Supporting Information) and evolves with a characteristic time that is similar to the disordered Raman bands (Figure 7a,c).

dx.doi.org/10.1021/bi500528x | Biochemistry 2014, 53, 6550−6565

DISCUSSION

The Need for Multiple Biophysical Probes to Study the Kinetics of Tau Fibril Formation. The process of amyloid fibril formation is known to be complex and heterogeneous.[83] It appears likely that even when the aggregation mechanism conforms to an NDP model, there will be multiple pathways for the formation of mature amyloid fibrils and each of these pathways will originate from a different prefibrillar precursor.[84,85] It has been hypothesized that the structural polymorphism observed in amyloid fibrils has its kinetic origins in multiple pathways for fibrillar growth.[84−88] Clearly, the interrogation of such a complex process requires the utilization of multiple biophysical probes since different probes have different sensitivities and limits of resolution.[89]

An earlier model for tau4RD aggregation in the presence of heparin, derived mainly from examining the protein and heparin concentration-dependences of ThT fluorescence-monitored aggregation kinetics concluded that the aggregation mechanism was best described by a ligand-induced NDP model.[14] In addition, the protein concentration-dependence of the aggregation kinetics enabled the existence of an off-pathway intermediate to be postulated.[14] The off-pathway intermediate formed a mixture of structures that included nonfibrillar aggregates and beaded protofibrils, as detected by AFM.[14] These structures disappeared, however, early in the aggregation reaction and over the rest of the time course of the aggregation reaction, the early fibrillar aggregates transformed into the final, mature fibrils.[14] Despite this complexity of structures observed using AFM, the ThT fluorescence kinetics were monophasic,[14] and no information was available about the specific secondary structural contents of the different species populated.

In this study, UVRR spectroscopy has been employed to study the kinetics of conformational conversion as disordered tau4RD monomer transforms into ordered, mature fibrils (Figures 4 and 5). The kinetics of structural evolution during aggregation has been studied by examining the changes in position (Figure 6) and the changes in intensity (Figure 7) of specific Raman bands that are known to denote particular classes of secondary structure, as a function of aggregation time. The interpretations of the change in intensity, in particular, have been done with the knowledge that although certain bands (1382 cm^{-1}, for example) predominantly arise from disordered conformations,[28−31,41,46] they are also known to be present to a lesser extent as shoulders in the UVRR spectra of β-sheet conformations.[29,61] Hence, the rate of change in intensity does not represent the rate of evolution of a particular conformation alone. The goal has been to correlate the characteristic times of secondary structural changes with the characteristic times of evolution of the two stages of fibrillization identified by the sedimentation assay and corroborated by the AFM measurements (Figures 2 and 3). Hence, multivariate statistical analyses of the data, such as 2D correlation analysis,[28,31] analysis of ψ dihedral angle distributions for the Am III region,[35,62] or analysis using basis spectra derived for the different classes of secondary structure, all of which require large data sets of spectra, have not been carried out in the present study.

Structural Conversion of Disordered Tau Monomer to Mature, Ordered Tau Fibrils. The aggregation reaction appears deceptively simple when monitored by ThT fluorescence, which increases in a single exponential manner as the reaction proceeds. The complexity of the aggregation reaction is, however, revealed by the UVRR spectra collected at different times during the aggregation process (Figure 5). Changes in the UVRR spectra are seen to occur in two stages. During stage I, the Am I band shifts downward in wavenumber from its position in the monomer in the absence of heparin to its position in the early fibrillar aggregates seen at 1 h. (Figure 6b). During stage II, it increases in wavenumber as the final mature fibrils form (Figure 6b). The 1382 and 1560 cm^{-1} bands that are signatures of disordered conformations decrease in intensity during stage I and thereafter increase in intensity during stage II (Figure 7a,c). This increase in the intensities of the 1382 and 1560 cm^{-1} Raman bands occurs concurrently with an increase in the intensity of ThT fluorescence (Figures 2a and 7d). Hence, UVRR spectroscopy yields information about the structural changes that occur when early fibrillar aggregates first form from monomer upon the addition of heparin, and when the early fibrillar aggregates transform more slowly into mature fibrils.

At the end of stage I (1 h), the Am I band position indicates that the early fibrillar aggregates (Figure 3b) present at this time possess β-sheet structure (Figure 6b). The decrease in intensity of the 1382 and 1560 cm^{-1} bands indicates that the early fibrillar aggregates possess less disordered content than the predominantly disordered monomer (Figure 7a,c) from which they arise. It is likely that this decrease in intensity arises from a change in the scattering cross sections of these Raman bands. Hence, the UVRR data indicate that the early fibrillar aggregates formed at the end of stage I have β-sheet structure not detectable in the monomer, which appears to have formed from some of the disordered conformations present in the monomer, following the addition of heparin.

As the fibrils mature from 1 to 24 h, the β-sheet content increases (Figures 6b and 7b). This increase in β-sheet content must occur at the cost of a decrease in the other conformations present in the early fibrillar aggregates seen at 1 h. The only other conformations that appear to be present in the early fibrillar aggregates are disordered conformations (see above), so these, in totality, must decrease during fibril maturation. The observation that the UVRR signatures for disorder, specifically the 1382 and 1560 cm^{-1} bands (Figure 7a,c), do not decrease but instead increase in intensity during stage II as fibrils mature with conformational change might therefore appear puzzling. But as described earlier, the UVRR signatures for disorder that are resonance enhanced in this study (λ_{exc} = 220 nm), namely, the bands positioned at 1382 and 1560 cm^{-1}, cannot distinguish between the different types of disorder, whether unordered structures, PPII or turns. Hence, it appears that although the disordered segments interspersed between the β-strands must decrease in length as β-sheet content increases during fibril maturation, a redistribution of conformations in these segments occurs, such that disordered conformations with higher Raman scattering cross sections at 1382 and 1560 cm^{-1} form, at the expense of disordered conformations with lower scattering cross sections. In this way, these Raman bands, which contain contributions from all three disordered conformations (unordered structures, PPII and turns), increase in intensity during stage II, even though the total amount of disorder must decrease.

Unfortunately, this UVRR spectroscopic study cannot distinguish between the disordered conformations that must differ in their Raman scattering cross sections. CD and FTIR spectra suggest that the disordered conformation in mature fibrils is random coil[22,64] (see Results), but ssNMR, HX-NMR, and EPR studies suggest they might be loops or turns[20−22,56]

dx.doi.org/10.1021/bi500528x | Biochemistry 2014, 53, 6550−6565

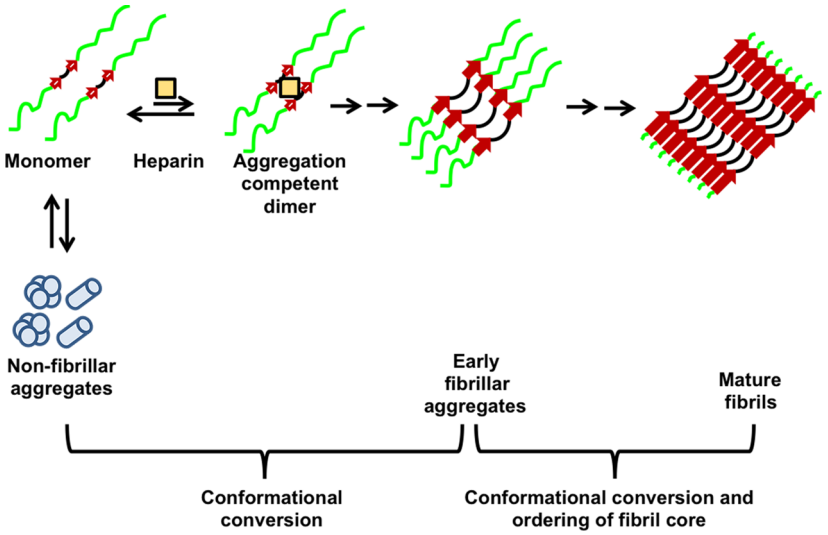

Figure 9. A minimal working model for the formation of fibrils by the repeat domain of tau in the presence of heparin, derived from this study of tau aggregation using multiple biophysical probes. Heparin is required primarily for the formation of the aggregation-competent dimer. Early fibrillar aggregates are seen to have formed at 1 h by the conformational conversion of the off-pathway, nonfibrillar aggregates. Fibril maturation occurs from the time they are first observed (1 h) up to 24 h. During fibril maturation, the processes of conformational conversion and the ordering of the fibril core occur concurrently. For all structures in cartoon representation, red arrows denote β-strands, black loops denote β-turns, and green squiggles denote unordered structures. During aggregation, there is an increased formation of β-sheet and disordered turns at the expense of a decrease in unordered structures. Mature fibrils are represented arbitrarily as structures that show parallel, in-register alignment of the β-strands (red arrows) without reference to any particular structural model. Although the ordering of the fibril core is depicted by the packing of β-strands within the β-sheet, the actual process may well correspond to the twisting/packing of the β-sheet bilayer.

(Figure 1b). Other studies on other proteins have demonstrated that the loops that connect the same or different secondary structural elements in proteins are present either as β-turns or as PPII.[67] It thus appears likely that the final tau fibril has disordered turns or PPII segments interspersed between the β-strands that compose the ordered β-sheet. It is hence proposed that as early fibrillar aggregates undergo internal structural change to form the final mature fibrils, the β-sheet conformation increases at the expense of a decrease in total disordered conformation, and that within the family of disordered conformations, the turn or PPII conformation increases at the expense of a decrease in unordered structures (Figure 9). Indeed, the simultaneous formation of turns and β-strands as monitored by the synchronous appearance of the 1377 and 1392 cm^{-1} Raman bands has been shown to be a part of the mechanism of fibril formation by YE8, a genetically engineered, intrinsically disordered polypeptide.[31]

Conformational Conversion and Consolidation of the Fibril Core Occur Concurrently. The characteristic time for conformational conversion as determined from the change in the Am III_3 band position (Figure 6a), the characteristic time for redistribution of disordered conformations as determined from the change in intensities of the 1382 and 1560 cm^{-1} bands (Figures 7a, c), the consolidation of the fibril core as measured by the characteristic time of change in the Am I band position from 1 h onward (Figure 6b) and by the characteristic time of change in the intensities of the 1402 and 1610 cm^{-1} bands (Figures 7b and 8) are all similar to the characteristic time for the evolution of ThT fluorescence (Figure 7d). Thus, it appears that the transformation of the early fibrillar aggregates into mature fibrils from 1 to 24 h is characterized by simultaneous conformational conversion and the consolidation of the fibril core (Figures 7d and 9). It is possible that the early fibrillar aggregates undergo molecular recycling during fibril maturation, as has been shown to be the case for other fibril-forming proteins.[90,91] The process of molecular recycling is not expected, however, to alter the number concentration of fibrils that has been inferred to remain approximately constant from 1 h onward (on the basis of the single exponential time course traced by all biophysical probes).

It is known that heparin, which has been used to induce tau aggregation, is not present in the mature tau fibril core.[14,55,71] It is likely that the heparin dissociates as the major secondary structural changes occur during fibril maturation from 1 to 10 h. This would be consistent with the primary kinetic role of heparin as an inducer of tau aggregation being to enable the formation of the aggregation-competent dimer, which serves as an aggregation nucleus,[14] to which monomers then add (Figure 9). At present it is not known whether it is the dissociation of heparin that drives the major structural changes or whether it is the major structural changes that drive the dissociation of heparin. Heparin does not contribute any Raman bands to the UVRR spectrum measured at 220 nm (Figure S5, Supporting Information), and hence, this change in bound versus free heparin is not visible using UVRR spectroscopy.

Significance of This Study. This is the first study to have examined the kinetics of tau fibril formation using UVRR spectroscopy as a probe. Changes in the UVRR spectra occur in two stages as the fibril formation reaction of tau progresses (Figure 9). The first stage corresponds to the changes in the UVRR spectra that accompany the formation of early fibrillar aggregates during the first 1 h. The second stage corresponds to changes in the UVRR spectra, from 1 to 24 h, accompanying the conformational conversion reactions that lead to the formation of mature fibrils with a consolidated cross-β core (Figures 3, 6, and 7). Indeed, studies of disease progression in AD have shown that there are two broad stages to tau pathology *in vivo* as well: the first stage involves the formation of nonfibrillar, dye-negative "pretangles" and the second stage involves the formation of the final, dye-positive, mature

neurofibrillary tangles.[92] The observations of two distinct stages of changes in the UVRR spectra during the formation of tau fibrils hence contribute toward the understanding of structural events that occur during the aggregation of tau. If future experiments can elucidate the toxicities of various species formed on the aggregation pathway, then the understanding gained from this study, of the structural content of the various species populated on the aggregation pathway, should enable the targeted design of inhibitory compounds[93] that prevent tau fibril formation. Lastly, this study has also demonstrated that the fluorescence of the dye ThT specifically measures the maturation of fibrils, on the basis of the similarity of the rates measured by the ThT fluorescence and UVRR spectroscopic probes (Figure 7d).

■ ASSOCIATED CONTENT

Supporting Information

Controls for UVRR spectral acquisition, FTIR spectra of tau fibrils, the kinetics of change in intensity of the 1463 cm^{-1} X-Pro Raman band, and UVRR spectrum of heparin. This material is available free of charge via the Internet at http://pubs.acs.org.

■ AUTHOR INFORMATION

Corresponding Authors

*J.B.U. E-mail: jayant@ncbs.res.in. Telephone: 91-80-23666150. Fax: 91-80-23636662.

*M.P. E-mail: mrinalini@iiserpune.ac.in. Telephone: 91-735-069-4600.

Present Addresses

[†]G.R.: Department of Molecular Biosciences, Northwestern University, Evanston, IL 60208, USA.

[‡]M.P.: Indian Institute of Science Education and Research, Pune 411008, India.

Funding

This work was funded by the Tata Institute of Fundamental Research and by the Department of Biotechnology, Government of India. G.R. was a recipient of the SP Mukherjee fellowship from the Council of Scientific and Industrial Research, Government of India at the time of this study. J.B.U. is a recipient of the JC Bose National Fellowship from the Government of India. M.P. is a recipient of the Innovative Young Biotechnologist Award (IYBA) from the Department of Biotechnology, Government of India.

Notes

The authors declare no competing financial interest.

■ ACKNOWLEDGMENTS

G.R. thanks Spriha Gogia, Namrata Jayanth, and Aniruddha Panda for help with initial experiments. The AFM images were acquired at the Central Imaging Facility of the National Centre for Biological Sciences.

■ ABBREVIATIONS

ThT, thioflavin T; NDP, nucleation-dependent polymerization; UVRR, ultraviolet resonance Raman; NMR, nuclear magnetic resonance; ssNMR, solid-state NMR; EPR, electron paramagnetic resonance; CD, circular dichroism; FTIR, Fourier transform infrared; AFM, atomic force microscopy; PPII, polyproline II; DTT, dithiothreitol; HX-MS, hydrogen−deuterium exchange coupled to mass spectrometry

■ REFERENCES

(1) Weingarten, M. D., Lockwood, A. H., Hwo, S. Y., and Kirschner, M. W. (1975) A protein factor essential for microtubule assembly. *Proc. Natl. Acad. Sci. U. S. A. 72*, 1858−1862.

(2) Schweers, O., Schonbrunn-Hanebeck, E., Marx, A., and Mandelkow, E. (1994) Structural studies of tau protein and Alzheimer paired helical filaments show no evidence for beta-structure. *J. Biol. Chem. 269*, 24290−24297.

(3) Mukrasch, M. D., Bibow, S., Korukottu, J., Jeganathan, S., Biernat, J., Griesinger, C., Mandelkow, E., and Zweckstetter, M. (2009) Structural polymorphism of 441-residue tau at single residue resolution. *PLoS Biol. 7*, No. e34.

(4) Ballatore, C., Lee, V. M., and Trojanowski, J. Q. (2007) Tau-mediated neurodegeneration in Alzheimer's disease and related disorders. *Nat. Rev. Neurosci. 8*, 663−672.

(5) Ramachandran, G., and Udgaonkar, J. B. (2013) Mechanistic studies unravel the complexity inherent in tau aggregation leading to Alzheimer's disease and the tauopathies. *Biochemistry 52*, 4107−4126.

(6) Lee, G., Cowan, N., and Kirschner, M. (1988) The primary structure and heterogeneity of tau protein from mouse brain. *Science 239*, 285−288.

(7) Gustke, N., Trinczek, B., Biernat, J., Mandelkow, E. M., and Mandelkow, E. (1994) Domains of tau protein and interactions with microtubules. *Biochemistry 33*, 9511−9522.

(8) Wischik, C. M., Novak, M., Edwards, P. C., Klug, A., Tichelaar, W., and Crowther, R. A. (1988) Structural characterization of the core of the paired helical filament of Alzheimer disease. *Proc. Natl. Acad. Sci. U. S. A. 85*, 4884−4888.

(9) Friedhoff, P., von Bergen, M., Mandelkow, E. M., Davies, P., and Mandelkow, E. (1998) A nucleated assembly mechanism of Alzheimer paired helical filaments. *Proc. Natl. Acad. Sci. U. S. A. 95*, 15712−15717.

(10) Goedert, M., Jakes, R., Spillantini, M. G., Hasegawa, M., Smith, M. J., and Crowther, R. A. (1996) Assembly of microtubule-associated protein tau into Alzheimer-like filaments induced by sulphated glycosaminoglycans. *Nature 383*, 550−553.

(11) Wilson, D. M., and Binder, L. I. (1997) Free fatty acids stimulate the polymerization of tau and amyloid beta peptides. In vitro evidence for a common effector of pathogenesis in Alzheimer's disease. *Am. J. Pathol. 150*, 2181−2195.

(12) Chirita, C. N., Necula, M., and Kuret, J. (2003) Anionic micelles and vesicles induce tau fibrillization in vitro. *J. Biol. Chem. 278*, 25644−25650.

(13) King, M. E., Ahuja, V., Binder, L. I., and Kuret, J. (1999) Ligand-dependent tau filament formation: implications for Alzheimer's disease progression. *Biochemistry 38*, 14851−14859.

(14) Ramachandran, G., and Udgaonkar, J. B. (2011) Understanding the kinetic roles of the inducer heparin and of rod-like protofibrils during amyloid fibril formation by Tau protein. *J. Biol. Chem. 286*, 38948−38959.

(15) Congdon, E. E., Kim, S., Bonchak, J., Songrug, T., Matzavinos, A., and Kuret, J. (2008) Nucleation-dependent tau filament formation: the importance of dimerization and an estimation of elementary rate constants. *J. Biol. Chem. 283*, 13806−13816.

(16) Necula, M., and Kuret, J. (2004) A static laser light scattering assay for surfactant-induced tau fibrillization. *Anal. Biochem. 333*, 205−215.

(17) Ramachandran, G., and Udgaonkar, J. B. (2012) Evidence for the Existence of a Secondary Pathway for Fibril Growth during the Aggregation of Tau. *J. Mol. Biol. 421*, 296−314.

(18) Berriman, J., Serpell, L. C., Oberg, K. A., Fink, A. L., Goedert, M., and Crowther, R. A. (2003) Tau filaments from human brain and from in vitro assembly of recombinant protein show cross-beta structure. *Proc. Natl. Acad. Sci. U. S. A. 100*, 9034−9038.

(19) Sawaya, M. R., Sambashivan, S., Nelson, R., Ivanova, M. I., Sievers, S. A., Apostol, M. I., Thompson, M. J., Balbirnie, M., Wiltzius, J. J., McFarlane, H. T., Madsen, A. O., Riekel, C., and Eisenberg, D. (2007) Atomic structures of amyloid cross-beta spines reveal varied steric zippers. *Nature 447*, 453−457.

(20) Margittai, M., and Langen, R. (2004) Template-assisted filament growth by parallel stacking of tau. *Proc. Natl. Acad. Sci. U. S. A. 101*, 10278−10283.
(21) Daebel, V., Chinnathambi, S., Biernat, J., Schwalbe, M., Habenstein, B., Loquet, A., Akoury, E., Tepper, K., Muller, H., Baldus, M., Griesinger, C., Zweckstetter, M., Mandelkow, E., Vijayan, V., and Lange, A. (2012) β-Sheet Core of Tau Paired Helical Filaments Revealed by Solid-State NMR. *J. Am. Chem. Soc. 134*, 13982−13989.
(22) Andronesi, O. C., von Bergen, M., Biernat, J., Seidel, K., Griesinger, C., Mandelkow, E., and Baldus, M. (2008) Characterization of Alzheimer's-like paired helical filaments from the core domain of tau protein using solid-state NMR spectroscopy. *J. Am. Chem. Soc. 130*, 5922−5928.
(23) Tompa, P. (2009) Structural disorder in amyloid fibrils: Its implication in dynamic interactions of proteins. *FEBS J. 276*, 5406−5415.
(24) Seshadri, S., Khurana, R., and Fink, A. L. (1999) Fourier transform infrared spectroscopy in analysis of protein deposits. *Methods Enzymol. 309*, 559−576.
(25) Woody, R. W. (1995) Circular dichroism. *Methods Enzymol. 246*, 34−71.
(26) Manning, M. C. (1989) Underlying assumptions in the estimation of secondary structure content in proteins by circular dichroism spectroscopy–a critical review. *J. Pharm. Biomed. Anal. 7*, 1103−1119.
(27) Soldi, G., Bemporad, F., Torrassa, S., Relini, A., Ramazzotti, M., Taddei, N., and Chiti, F. (2005) Amyloid formation of a protein in the absence of initial unfolding and destabilization of the native state. *Biophys. J. 89*, 4234−4244.
(28) Shashilov, V. A., and Lednev, I. K. (2008) 2D correlation deep UV resonance raman spectroscopy of early events of lysozyme fibrillation: kinetic mechanism and potential interpretation pitfalls. *J. Am. Chem. Soc. 130*, 309−317.
(29) Chi, Z., Chen, X. G., Holtz, J. S., and Asher, S. A. (1998) UV resonance Raman-selective amide vibrational enhancement: quantitative methodology for determining protein secondary structure. *Biochemistry 37*, 2854−2864.
(30) Huang, C. Y., Balakrishnan, G., and Spiro, T. G. (2006) Protein secondary structure from deep-UV resonance Raman spectroscopy. *J. Raman Spectrosc. 37*, 277−282.
(31) Sikirzhytski, V., Topilina, N. I., Takor, G. A., Higashiya, S., Welch, J. T., Uversky, V. N., and Lednev, I. K. (2012) Fibrillation mechanism of a model intrinsically disordered protein revealed by 2D correlation deep UV resonance Raman spectroscopy. *Biomacromolecules 13*, 1503−1509.
(32) Barghorn, S., and Mandelkow, E. (2002) Toward a unified scheme for the aggregation of tau into Alzheimer paired helical filaments. *Biochemistry 41*, 14885−14896.
(33) Jayanth, N., Ramachandran, S., and Puranik, M. (2009) Solution structure of the DNA damage lesion 8-oxoguanosine from ultraviolet resonance Raman spectroscopy. *J. Phys. Chem. A 113*, 1459−1471.
(34) Gonzalez-Montalban, N., Makarava, N., Savtchenko, R., and Baskakov, I. V. (2011) Relationship between conformational stability and amplification efficiency of prions. *Biochemistry 50*, 7933−7940.
(35) Popova, L. A., Kodali, R., Wetzel, R., and Lednev, I. K. (2010) Structural variations in the cross-beta core of amyloid beta fibrils revealed by deep UV resonance Raman spectroscopy. *J. Am. Chem. Soc. 132*, 6324−6328.
(36) Fodor, S. P. A., Copeland, R. A., Grygon, C. A., and Spiro, T. G. (1989) Deep-Ultraviolet Raman Excitation Profiles and Vibronic Scattering Mechanisms of Phenylalanine, Tyrosine, and Tryptophan. *J. Am. Chem. Soc. 111*, 5509−5518.
(37) Wang, Y., Purrello, R., Jordan, T., and Spiro, T. G. (1991) UVRR Spectroscopy of the Peptide Bond. 1. Amide S, a Nonhelical Structure Marker, Is a $C_\alpha H$ Bending Mode. *J. Am. Chem. Soc. 113*, 6359−6368.
(38) Mikhonin, A. V., Ahmed, Z., Ianoul, A., and Asher, S. A. (2004) Assignments and conformational dependencies of the amide III peptide backbone UV resonance Raman bands. *J. Phys. Chem. B 108*, 19020−19028.
(39) Xu, M., Shashilov, V., and Lednev, I. K. (2007) Probing the cross-β core structure of amyloid fibrils by hydrogen-deuterium exchange deep ultraviolet resonance Raman spectroscopy. *J. Am. Chem. Soc. 129*, 11002−11003.
(40) Maiti, N. C., Apetri, M. M., Zagorski, M. G., Carey, P. R., and Anderson, V. E. (2004) Raman spectroscopic characterization of secondary structure in natively unfolded proteins: α-Synuclein. *J. Am. Chem. Soc. 126*, 2399−2408.
(41) JiJi, R. D., Balakrishnan, G., Hu, Y., and Spiro, T. G. (2006) Intermediacy of poly(L-proline) II and β-strand conformations in poly(L-lysine) β-sheet formation probed by temperature-jump/UV resonance Raman spectroscopy. *Biochemistry 45*, 34−41.
(42) Roach, C. A., Simpson, J. V., and JiJi, R. D. (2012) Evolution of quantitative methods in protein secondary structure determination via deep-ultraviolet resonance Raman spectroscopy. *Analyst 137*, 555−562.
(43) Oladepo, S. A., Xiong, K., Hong, Z., Asher, S. A., Handen, J., and Lednev, I. K. (2012) UV resonance Raman investigations of peptide and protein structure and dynamics. *Chem. Rev. 112*, 2604−2628.
(44) Takeuchi, H., and Harada, I. (1990) Ultraviolet resonance Raman-spectroscopy of X-Proline bonds - a new marker band of hydrogen-bonding at the imide C═O site. *J. Raman Spectrosc. 21*, 509−515.
(45) Jordan, T., Mukerji, I., Wang, Y., and Spiro, T. G. (1996) UV resonance Raman spectroscopy and hydrogen bonding of the proline peptide bond. *J. Mol. Struct. 379*, 51−64.
(46) Austin, J. C., Jordan, T., and Spiro, T. G. (1993) *Ultraviolet Resonance Raman Studies of Proteins and Related Model Compounds*, Wiley & Sons Ltd., New York.
(47) Ramachandran, G., and Udgaonkar, J. B. (2013) Difference in fibril core stability between two tau four-repeat domain proteins: a hydrogen-deuterium exchange coupled to mass spectrometry study. *Biochemistry 52*, 8787−8789.
(48) Naiki, H., Higuchi, K., Hosokawa, M., and Takeda, T. (1989) Fluorometric determination of amyloid fibrils in vitro using the fluorescent dye, thioflavin T1. *Anal. Biochem. 177*, 244−249.
(49) LeVine, H., 3rd. (1993) Thioflavine T interaction with synthetic Alzheimer's disease beta-amyloid peptides: Detection of amyloid aggregation in solution. *Protein Sci. 2*, 404−410.
(50) Biancalana, M., Makabe, K., Koide, A., and Koide, S. (2009) Molecular mechanism of thioflavin-T binding to the surface of beta-rich peptide self-assemblies. *J. Mol. Biol. 385*, 1052−1063.
(51) Kitts, C. C., and Vanden Bout, D. A. (2009) Near-field scanning optical microscopy measurements of fluorescent molecular probes binding to insulin amyloid fibrils. *J. Phys. Chem. B 113*, 12090−12095.
(52) Chirita, C. N., Congdon, E. E., Yin, H., and Kuret, J. (2005) Triggers of full-length tau aggregation: A role for partially folded intermediates. *Biochemistry 44*, 5862−5872.
(53) Mukrasch, M. D., Biernat, J., von Bergen, M., Griesinger, C., Mandelkow, E., and Zweckstetter, M. (2005) Sites of tau important for aggregation populate β-structure and bind to microtubules and polyanions. *J. Biol. Chem. 280*, 24978−24986.
(54) Mukrasch, M. D., Markwick, P., Biernat, J., Bergen, M., Bernado, P., Griesinger, C., Mandelkow, E., Zweckstetter, M., and Blackledge, M. (2007) Highly populated turn conformations in natively unfolded tau protein identified from residual dipolar couplings and molecular simulation. *J. Am. Chem. Soc. 129*, 5235−5243.
(55) von Bergen, M., Barghorn, S., Muller, S. A., Pickhardt, M., Biernat, J., Mandelkow, E. M., Davies, P., Aebi, U., and Mandelkow, E. (2006) The core of tau-paired helical filaments studied by scanning transmission electron microscopy and limited proteolysis. *Biochemistry 45*, 6446−6457.
(56) Margittai, M., and Langen, R. (2006) Side chain-dependent stacking modulates tau filament structure. *J. Biol. Chem. 281*, 37820−37827.
(57) Song, S., and Asher, S. A. (1989) UV resonance Raman studies of peptide conformation in poly(L-lysine), poly(L-glutamic acid), and

model complexes: The basis for protein secondary structure determinations. *J. Am. Chem. Soc. 111*, 4295−4305.
(58) Copeland, R. A., and Spiro, T. G. (1987) Secondary structure determination in proteins from deep (192−223-nm) ultraviolet Raman spectroscopy. *Biochemistry 26*, 2134−2139.
(59) Chen, X. G., Asher, S. A., Schweitzer-Stenner, R., Mirkin, N. G., and Krimm, S. (1995) UV Raman Determination of the $\pi\cdots\pi^*$ Excited State Geometry of *N*-Methylacetamide: Vibrational Enhancement Pattern. *J. Am. Chem. Soc. 117*, 2884−2895.
(60) Wang, Y., Purrello, R., Georgiou, S., and Spiro, T. G. (1991) UVRR spectroscopy of the peptide bond. 2. Carbonyl H-bond effects on the ground- and excited-state structures of *N*-methylacetamide. *J. Am. Chem. Soc. 113*, 6368−6377.
(61) Balakrishnan, G., Hu, Y., and Spiro, T. G. (2012) His26 protonation in cytochrome c triggers microsecond β-sheet formation and heme exposure: Implications for apoptosis. *J. Am. Chem. Soc. 134*, 19061−19069.
(62) Sikirzhytski, V., Topilina, N. I., Higashiya, S., Welch, J. T., and Lednev, I. K. (2008) Genetic engineering combined with deep UV resonance Raman spectroscopy for structural characterization of amyloid-like fibrils. *J. Am. Chem. Soc. 130*, 5852−5853.
(63) Wang, M., and Jiji, R. D. (2011) Spectroscopic detection of beta-sheet structure in nascent Abeta oligomers. *J. Biophotonics 4*, 637−644.
(64) Barghorn, S., Davies, P., and Mandelkow, E. (2004) Tau paired helical filaments from Alzheimer's disease brain and assembled in vitro are based on β-structure in the core domain. *Biochemistry 43*, 1694−1703.
(65) Asher, S. A., Mikhonin, A. V., and Bykov, S. (2004) UV Raman demonstrates that α-helical polyalanine peptides melt to polyproline II conformations. *J. Am. Chem. Soc. 126*, 8433−8440.
(66) Shi, Z., Chen, K., Liu, Z., and Kallenbach, N. R. (2006) Conformation of the backbone in unfolded proteins. *Chem. Rev. 106*, 1877−1897.
(67) Fitzkee, N. C., Fleming, P. J., Gong, H., Panasik, N., Jr., Street, T. O., and Rose, G. D. (2005) Are proteins made from a limited parts list? *Trends Biochem. Sci. 30*, 73−80.
(68) Syme, C. D., Blanch, E. W., Holt, C., Jakes, R., Goedert, M., Hecht, L., and Barron, L. D. (2002) A Raman optical activity study of rheomorphism in caseins, synucleins and tau. New insight into the structure and behaviour of natively unfolded proteins. *Eur. J. Biochem. 269*, 148−156.
(69) von Bergen, M., Barghorn, S., Biernat, J., Mandelkow, E. M., and Mandelkow, E. (2005) Tau aggregation is driven by a transition from random coil to beta sheet structure. *Biochim. Biophys. Acta 1739*, 158−166.
(70) Zhu, H. L., Fernandez, C., Fan, J. B., Shewmaker, F., Chen, J., Minton, A. P., and Liang, Y. (2010) Quantitative characterization of heparin binding to Tau protein: Implication for inducer-mediated Tau filament formation. *J. Biol. Chem. 285*, 3592−3599.
(71) Carlson, S. W., Branden, M., Voss, K., Sun, Q., Rankin, C. A., and Gamblin, T. C. (2007) A complex mechanism for inducer mediated tau polymerization. *Biochemistry 46*, 8838−8849.
(72) Elbaum-Garfinkle, S., and Rhoades, E. (2012) Identification of an aggregation-prone structure of tau. *J. Am. Chem. Soc. 134*, 16607−16613.
(73) Wegmann, S., Scholer, J., Bippes, C. A., Mandelkow, E., and Muller, D. J. (2011) Competing interactions stabilize pro- and anti-aggregant conformations of human Tau. *J. Biol. Chem. 286*, 20512−20524.
(74) von Bergen, M., Friedhoff, P., Biernat, J., Heberle, J., Mandelkow, E. M., and Mandelkow, E. (2000) Assembly of tau protein into Alzheimer paired helical filaments depends on a local sequence motif ((306)VQIVYK(311)) forming beta structure. *Proc. Natl. Acad. Sci. U. S. A. 97*, 5129−5134.
(75) Mikhonin, A. V., Bykov, S. V., Myshakina, N. S., and Asher, S. A. (2006) Peptide secondary structure folding reaction coordinate: Correlation between UV Raman amide III frequency, Ψ Ramachandran angle, and hydrogen bonding. *J. Phys. Chem. B 110*, 1928−1943.
(76) Chirgadze, Y. N., and Nevskaya, N. A. (1976) Infrared spectra and resonance interaction of amide-I vibration of the antiparallel-chain pleated sheet. *Biopolymers 15*, 607−625.
(77) Apetri, M. M., Maiti, N. C., Zagorski, M. G., Carey, P. R., and Anderson, V. E. (2006) Secondary structure of alpha-synuclein oligomers: characterization by raman and atomic force microscopy. *J. Mol. Biol. 355*, 63−71.
(78) Xiong, K., Punihaole, D., and Asher, S. A. (2012) UV resonance Raman spectroscopy monitors polyglutamine backbone and side chain hydrogen bonding and fibrillization. *Biochemistry 51*, 5822−5830.
(79) Chang, S., Yang, W., and Spiro, T. G. (1990) Saturation effects on ultraviolet resonance Raman intensities - excimer/YAG laser comparison and aromatic amino-acid cross-sections. *J. Raman Spectrosc. 21*, 435−440.
(80) Chi, Z. H., and Asher, S. A. (1998) UV Raman determination of the environment and solvent exposure of Tyr and Trp residues. *J. Phys. Chem. B 102*, 9595−9602.
(81) Moore, C. L., Huang, M. H., Robbennolt, S. A., Voss, K. R., Combs, B., Gamblin, T. C., and Goux, W. J. (2011) Secondary nucleating sequences affect kinetics and thermodynamics of tau aggregation. *Biochemistry 50*, 10876−10886.
(82) Kurouski, D., Deckert-Gaudig, T., Deckert, V., and Lednev, I. K. (2012) Structure and Composition of Insulin Fibril Surfaces Probed by TERS. *J. Am. Chem. Soc. 134*, 13323−13329.
(83) Toyama, B. H., and Weissman, J. S. (2011) Amyloid structure: Conformational diversity and consequences. *Annu. Rev. Biochem. 80*, 557−585.
(84) Kumar, S., and Udgaonkar, J. B. (2010) Mechanisms of amyloid fibril formation by proteins. *Curr. Sci. India 98*, 639−656.
(85) Goldsbury, C., Frey, P., Olivieri, V., Aebi, U., and Muller, S. A. (2005) Multiple assembly pathways underlie amyloid-beta fibril polymorphisms. *J. Mol. Biol. 352*, 282−298.
(86) Kumar, S., Mohanty, S. K., and Udgaonkar, J. B. (2007) Mechanism of formation of amyloid protofibrils of barstar from soluble oligomers: evidence for multiple steps and lateral association coupled to conformational conversion. *J. Mol. Biol. 367*, 1186−1204.
(87) Kumar, S., and Udgaonkar, J. B. (2009) Conformational conversion may precede or follow aggregate elongation on alternative pathways of amyloid protofibril formation. *J. Mol. Biol. 385*, 1266−1276.
(88) Jayaraman, M., Mishra, R., Kodali, R., Thakur, A. K., Koharudin, L. M., Gronenborn, A. M., and Wetzel, R. (2012) Kinetically competing huntingtin aggregation pathways control amyloid polymorphism and properties. *Biochemistry 51*, 2706−2716.
(89) Morris, A. M., Watzky, M. A., and Finke, R. G. (2009) Protein aggregation kinetics, mechanism, and curve-fitting: A review of the literature. *Biochim. Biophys. Acta 1794*, 375−397.
(90) Carulla, N., Caddy, G. L., Hall, D. R., Zurdo, J., Gairi, M., Feliz, M., Giralt, E., Robinson, C. V., and Dobson, C. M. (2005) Molecular recycling within amyloid fibrils. *Nature 436*, 554−558.
(91) Sanchez, L., Madurga, S., Pukala, T., Vilaseca, M., Lopez-Iglesias, C., Robinson, C. V., Giralt, E., and Carulla, N. (2011) Aβ40 and Aβ42 amyloid fibrils exhibit distinct molecular recycling properties. *J. Am. Chem. Soc. 133*, 6505−6508.
(92) Kuret, J., Chirita, C. N., Congdon, E. E., Kannanayakal, T., Li, G., Necula, M., Yin, H., and Zhong, Q. (2005) Pathways of tau fibrillization. *Biochim. Biophys. Acta 1739*, 167−178.
(93) Sievers, S. A., Karanicolas, J., Chang, H. W., Zhao, A., Jiang, L., Zirafi, O., Stevens, J. T., Munch, J., Baker, D., and Eisenberg, D. (2011) Structure-based design of non-natural amino-acid inhibitors of amyloid fibril formation. *Nature 475*, 96−100.